Journal of Orthopaedic Surgery and Research

RESEARCH

Open Access

Demineralized bone matrix combined with concentrated growth factors promotes intervertebral fusion in a novel rat extreme lateral interbody fusion model

Han Wu[1], Shaorong Li[1], WeiJian Wang[1], Jiaqi Li[1] and Wei Zhang[1*]

Abstract

Background Whether demineralized bone matrix (DBM) combined with concentrated growth factors (CGF) can accelerate intervertebral fusion remains uncertain. This study developed a novel rat model for extreme lateral interbody fusion (XLIF) and evaluated the fusion outcomes of DBM combined with CGF using imaging and histological analysis.

Methods A total of 70 male SD rats (3 months old, average body weight 300 ± 50 g) were included in this study. Among them, 10 rats were used for the anatomical study of the lumbar spine. The remaining 48 rats were randomly divided into four groups ($n = 12$ per group): Group A (control), Group B (titanium plate fixation), Group C (DBM + titanium plate fixation), and Group D (DBM + CGF + titanium plate fixation). The remaining 12 rats were used as donors to prepare fresh CGF. Eight weeks after surgery, the rats were euthanized and lumbar spine specimens were collected, with interbody fusion evaluated by manual palpation. Subsequently, specimens from groups B, C, and D were analyzed by micro-CT and histological examinations to comprehensively assess the fusion outcome.

Results The anatomical and surgical techniques for the rat XLIF model are described. Titanium plates (7 mm × 2.5 mm × 0.8 mm) and screws (3 mm × 1 mm) were designed based on the anatomical measurements. In Group A, spontaneous fusion occurred in 1 case; the remaining 11 cases showed intervertebral mobility. In Group B, 3 cases achieved fusion; in Group C, 8 cases; and in Group D, 11 cases. Micro-CT revealed fusion index scores (FIS) of 2.21 ± 0.51 for Group B, 3.62 ± 0.67 for Group C, and 4.57 ± 0.56 for Group D. Histological examination showed limited bone formation in Group B, with fibrous connective tissue filling the intervertebral space. Group C showed more bone formation, but some cartilage and fibrous tissue remained. Group D demonstrated abundant new bone formation and robust histological fusion, with substantial bridging between vertebrae.

First Author: Han Wu

*Correspondence:
Wei Zhang
37300332@hebmu.edu.cn

Full list of author information is available at the end of the article

Conclusion The rat XLIF model for interbody fusion has been successfully established and validated. Using this model, it was preliminarily demonstrated that DBM combined with CGF can effectively promote intervertebral fusion in rats.

Keywords Intervertebral fusion, XLIF, Concentrated growth factor, Demineralized bone matrix

Introduction

XLIF, an advanced minimally invasive spinal surgical technique, has been widely applied to the treatment of various degenerative lumbar diseases, such as spondylolisthesis, discogenic low back pain, and spinal stenosis [1]. Compared with traditional posterior lumbar approaches, XLIF accesses the intervertebral space via a retroperitoneal lateral route, avoiding interference with the lamina, nerve roots, and paraspinal muscles. This significantly reduces intraoperative soft tissue damage and postoperative pain, thereby shortening recovery time [2]. Moreover, XLIF allows for the implantation of larger interbody cages, providing increased bone contact area and more effective restoration of disc height, ultimately improving fusion rates and surgical outcomes [3]. As a result, XLIF has become an important minimally invasive technique for managing degenerative lumbar conditions. Despite its advantages, XLIF still faces challenges such as interbody fusion failure, cage subsidence, and adjacent segment degeneration, all of which can significantly compromise long-term outcomes [4]. To overcome these challenges, researchers have been actively exploring suitable biomaterials to enhance interbody fusion. Effective bone grafting remains critical in spinal surgery, with autografts and allografts being the most commonly used materials [5]. Among them, autogenous bone is considered the gold standard due to its superior osteoinductive, osteoconductive, and osteogenic properties. However, its use is limited by donor site morbidity and restricted graft availability [6]. Allografts, on the other hand, carry risks of immune rejection and disease transmission, and typically exhibit weaker osteoinductivity [7].

Against this background, DBM, a widely used bone substitute, has been increasingly applied in spinal fusion procedures. By removing the inorganic components of bone tissue, DBM retains organic elements such as collagen and certain growth factors, thereby endowing it with favorable osteoconductive properties and moderate osteoinductive potential [8]. However, compared to autogenous bone, DBM still lacks sufficient osteoinductivity, particularly in poorly vascularized intervertebral environments, rendering its fusion efficacy somewhat controversial [9]. CGF first developed by Sacco in 2005 using a variable-speed centrifugation technique applied to fresh whole blood, is a third-generation platelet concentrate widely used in tissue repair and bone regeneration [10]. As a third-generation platelet concentrate, CGF comprise a fibrin network abundant in growth factors, derived from autologous blood through specialized centrifugation protocols, and are widely employed in regenerative therapie. Compared with previous generations of platelet concentrates, such as platelet-rich plasma (PRP) and platelet-rich fibrin (PRF), CGF demonstrates superior biological performance in promoting bone regeneration. This superiority is mainly attributed to its high concentrations of active growth factors, including PDGF, TGF-β, VEGF, IGF-1 and BMPs [11, 12]. Additionally, CGF forms a densely cross-linked fibrin matrix that not only acts as a stable carrier for growth factors but also enables their sustained release, providing continuous biological stimulation for tissue repair [13]. Its abundance of growth factors and sustained-release capability endow CGF with significant advantages in tissue repair and bone regeneration.

Theoretically, the osteoinductive capacity of CGF, combined with the osteoconductive properties of DBM, may produce a synergistic effect by providing both a physical scaffold for cell adhesion and growth and sustained biological signals for bone healing, thereby enhancing intervertebral fusion outcomes. However, current studies on the combined application of CGF and DBM in spinal fusion remain limited, and reliable small-animal models for systematically verifying their effects are lacking. To the best of our knowledge, a small animal model that accurately simulates the clinical intervertebral fusion process has not yet been established [14]. Therefore, the aim of this study is to develop a novel rat lumbar interbody fusion model based on XLIF techniques and to evaluate the effect of CGF combined with DBM on intervertebral bone healing. Multidimensional evaluations, including imaging, histology, and immunohistochemistry, were conducted to validate the potential of this combination in promoting spinal fusion, thereby providing experimental evidence for future clinical material selection and mechanistic studies. Specifically, the objectives of this study are: (1) to characterize the anatomical features of the rat lumbar spine relevant to the XLIF approach and establish a clinically relevant rat interbody fusion model; (2) to investigate the efficacy of CGF combined with DBM in promoting lumbar interbody fusion using this model.

Materials and methods

Ethical support

All studies have been performed in accordance with the ethical standards in the 1964 Declaration of Helsinki and the relevant regulations of the US Health Insurance

Portability and Accountability Act (HIPAA). This experiment obtained ethical approval from the Ethics Committee of the Third Hospital of Hebei Medical University (No. Z2023-026-1).

Experimental animals and grouping

Seventy healthy adult male SPF SD rats (3 months old, 300 ± 50 g) were used and maintained under standard conditions (12-hour light/dark cycle, 25 °C, with free access to food and water). The study consisted of two parts: 1.Anatomical Study: Ten rats were euthanized for conventional lumbar CT scanning and anatomical observation. A fusion protocol was developed, and titanium plates and screws were designed to fit the rat anatomical structure. 2.Validation of the Interbody Fusion Model: Forty-eight rats were randomly assigned to four groups: Group A (control), Group B (titanium plate fixation), Group C (DBM + titanium plate fixation), and Group D (DBM + CGF + titanium plate fixation). Group A received only the surgical approach to the intervertebral space without fusion or titanium plate fixation. Group B underwent lateral titanium plate fixation without interbody fusion. Groups C and D underwent interbody fusion with lateral titanium plate fixation, using different intervertebral graft materials. Twelve rats were used as CGF donors.At 8 weeks postoperatively, all rats were euthanized for gross examination and manual palpation. Groups B, C, and D also underwent imaging and histological evaluations. Six rats from each group were selected for imaging, while the remaining six were used for histological staining and immunohistochemistry (Fig. 1).

Anatomical study

Ten skeletally mature 3-month-old male SD rats, with an average body weight of 300 ± 50 g, were selected for the study. First, under anesthesia with sodium pentobarbital (30 mg/kg, intraperitoneal injection), conventional lumbar computed tomography (CT) scans were performed to measure key anatomical parameters, including the maximum diameters of the vertebral body in the sagittal and coronal planes, the angle between the vertebral body and the transverse process, the lateral length of the vertebral body, and the maximum depth of the screw trajectory. After the completion of the CT scan, the rats were euthanized with an overdose of sodium pentobarbital (150 mg/

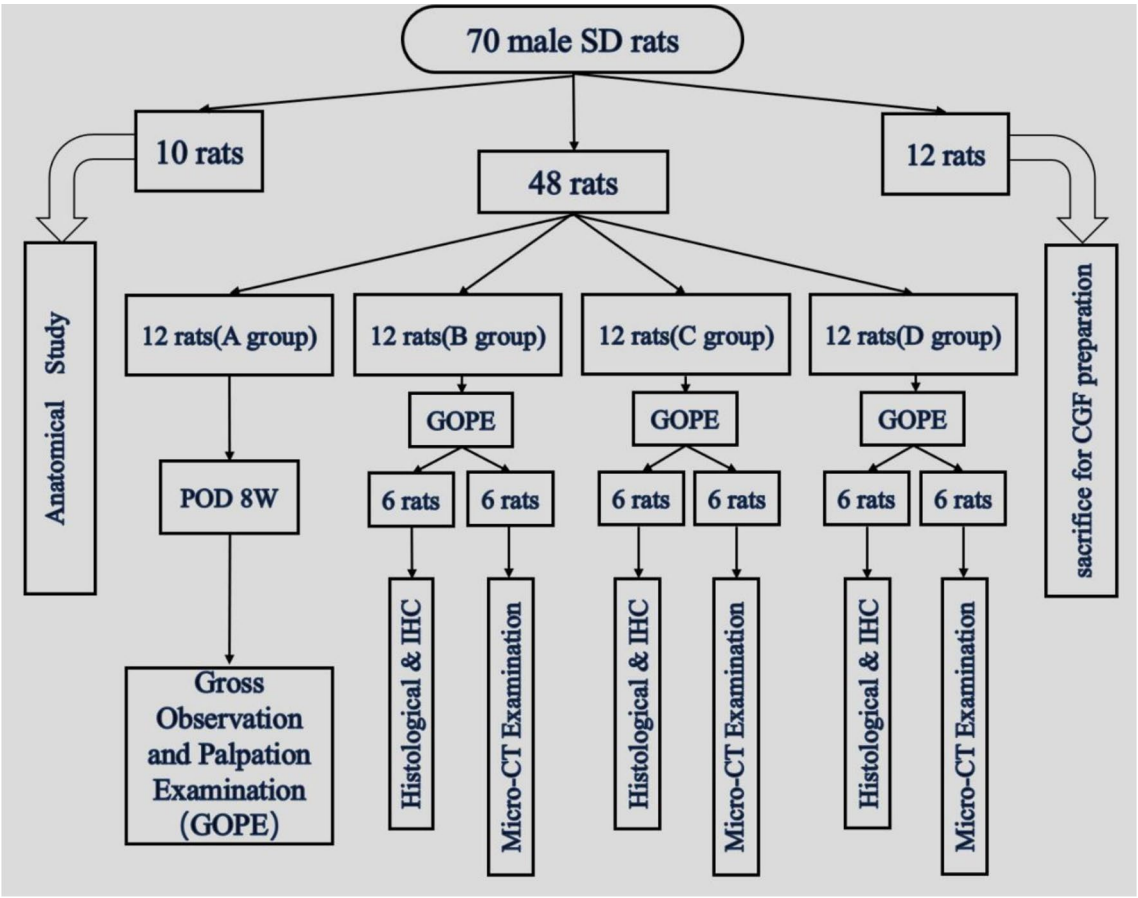

Fig. 1 Flow diagram of the study design indicating the group allocations and study procedures. **A**: control group; **B**:titanium plate fixation group; **C**:DBM + titanium plate fixation group; **D**:DBM + CGF + titanium plate fixation group. IHC:Immunohistochemistry

kg, intraperitoneal injection). A systematic dissection of the lumbar region was then performed to observe and document the anatomical features of the bones, soft tissues, and fascia related to intervertebral fusion.

Preparation of DBM

The DBM used in this study was sourced from Wright Medical Technology, Inc., provided in the form of ALLOMATRIX injectable DBM composite material. ALLOMATRIX contains DBM derived from humans, with components including demineralized bone filler powder, hydrated calcium sulfate, and sterile aqueous solution. When used, the DBM powder is mixed with water to form a putty-like substance, which can be molded freely according to the surgical requirements.

Preparation of CGF

Under isoflurane anesthesia, approximately 7 milliliters of blood was drawn from the heart of a pre-prepared allogenic donor rat and placed into a sterile glass tube (without the addition of anticoagulants). The sample was then subjected to automatic variable-speed centrifugation using a specialized device. The specific procedure was as follows: an initial acceleration for 30 s; followed by centrifugation at 2700 rpm (600 g) for 2 min; then at 2400 rpm (500 g) for 4 min; followed again by 2700 rpm for 4 min; then 3000 rpm (800 g) for 3 min; and finally, deceleration over 36 s until a complete stop. After centrifugation, the blood separated into three distinct layers: the upper layer was platelet-poor plasma (PPP), the middle layer was the CGF layer, and the bottom layer consisted of red blood cells (RBCs)(Fig. 2A-C). Studies have shown that the majority of active factors and CD34-positive cells within the centrifuge tube are primarily concentrated at the interface between the CGF layer and the RBC layer. Therefore, the CGF layer should include approximately the top 1 mm of the red blood cell layer [15]. The microstructure of the fibrin network in

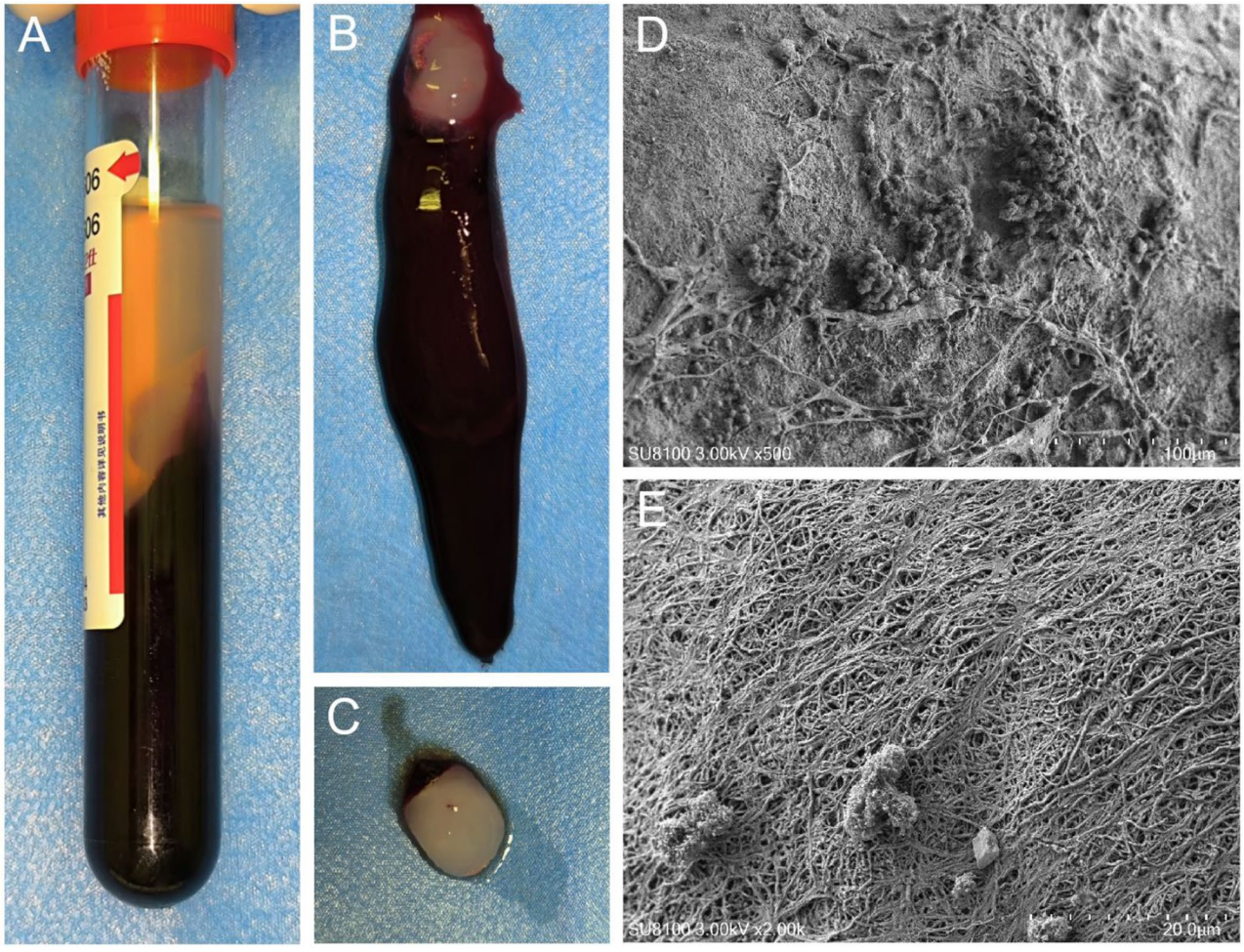

Fig. 2 Macroscopic examination and SEM analysis of CGF. **A**-**C**:The macroscopic appearance of CGF shows a three-layer structure in the collection tube: the top plasma layer, the middle yellow gel-like CGF layer, and the bottom red blood cell layer. **D**, **E**: SEM images at different magnifications reveal a dense fibrin network structure within the CGF

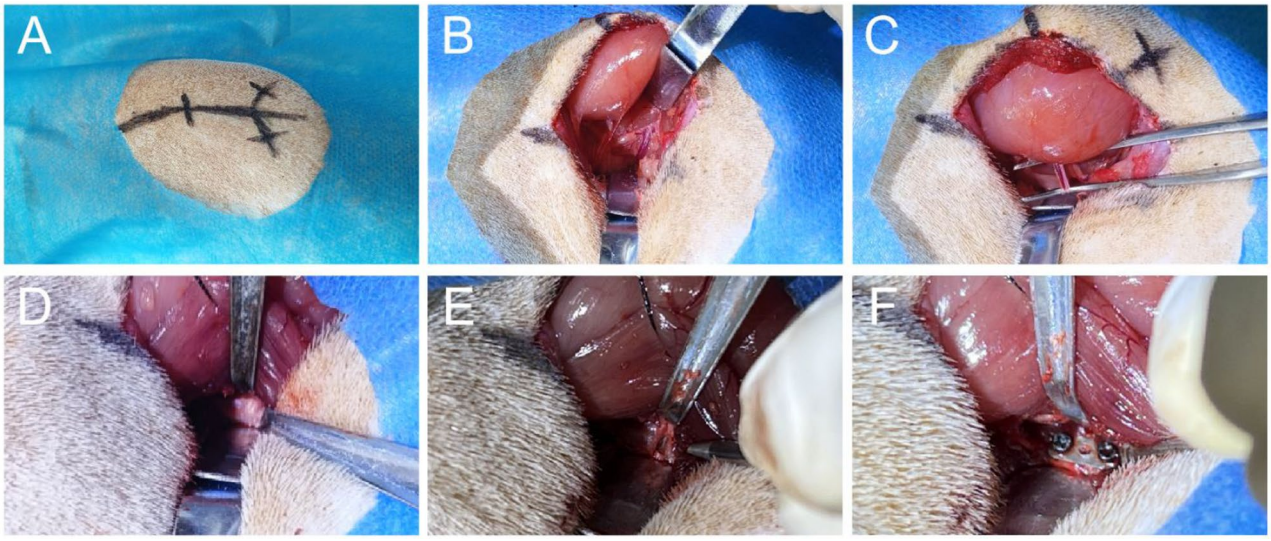

Fig. 3 Surgical procedure **A**: Surface landmarks were identified and marked. **B**: The surgical field was exposed. **C**: The iliac vessels were dissected and ligated. **D**: The intervertebral disc at the surgical segment was exposed. **E**: The intervertebral space was prepared. **F**: Lateral titanium plate fixation was applied

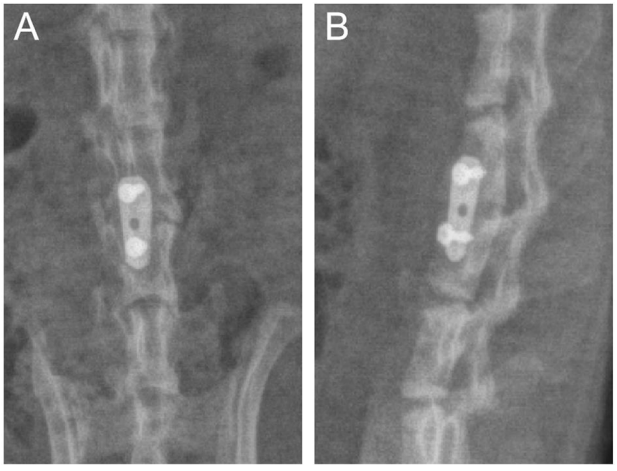

Fig. 4 Postoperative X-ray images of the rat lumbar spine in both anteroposterior (AP) and lateral views showed that the titanium plate and screws were properly positioned. The titanium plate was placed at the anterolateral aspect of the vertebral body, and the screws did not penetrate the spinal canal. **A**: Anteroposterior view **B**: Lateral view

CGF was further examined using SEM. This network is formed by the conversion of fibrinogen into fibrin during the coagulation process. The SEM image shows that CGF presents a complex structure composed of a dense fibrin network, platelets, and red blood cells (Fig. 2D, E).

Surgical procedure

Anesthesia was induced with 5% isoflurane in room air (300 ml/min) and maintained at 2% via a face mask. Depth was monitored by applying pressure to the tail, ears, or hind limbs, and adjusted as needed. After confirmation, the rat was placed in the right lateral decubitus position and fixed to the operating table. The lumbar area was shaved, disinfected with povidone-iodine, and draped (Fig. 3A). The L4-5 intervertebral space was located and marked based on the iliac crest (aligned with L6). A 4 cm curved incision was made 3–4 cm lateral to the spine. The external oblique, internal oblique, and transverse abdominal muscles were incised to expose the quadratus lumborum and retroperitoneal fat (Fig. 3B). Blunt dissection exposed the psoas muscle and iliac vessels, which were ligated (Fig. 3C). The abdominal aorta was used as a landmark. After exposing the lumbar spine and identifying the disc, the L4-5 disc was incised, and the nucleus pulposus was removed with a custom curette (Fig. 3D, E). Endplates were prepared by light sanding until slight bleeding occurred. The mixture of 0.2 ml DBM and 0.2 ml CGF was implanted into the intervertebral disc space, followed by lateral fixation of the surgical segment using titanium plates and screws (Fig. 3F). Proper placement of the internal fixation was confirmed under fluoroscopic X-ray imaging upon completion of the procedure (Fig. 4). Bleeding was checked, and the wound was closed in layers. The skin was disinfected, covered with sterile gauze, and bandaged. To prevent infection, 8U of sodium penicillin was administered intraperitoneally for 3 days. Postoperative monitoring included general condition, appetite, mobility, and signs of infection or urinary/fecal retention.

Gross observation and palpation examination

Two months post-surgery, the rats were euthanized, and the lumbar surgical segments were harvested. After removing surrounding soft tissues, X-rays were taken in anteroposterior and lateral views to evaluate internal fixation placement. The titanium plates and screws were then removed. Two blinded spine surgeons manually

assessed intervertebral motion by applying hyperextension and flexion to the fused segment.

Micro-CT examination

The lumbar vertebral tissue samples from the rats, which were fixed and preserved, were removed from the fixative, and the surfaces of the specimens were dried. The samples were then wrapped in plastic film and scanned using the SkyScan 1176 micro-CT imaging system (Bruker, Germany). The scan resolution was 18 μm, with a voltage of 65 kV, a current of 385 μA, and an exposure time of 340 ms, performing a full 360° scan. The image reconstruction software used was Dataviewer, and 3D reconstructions were generated using CTvox. The CTAn analysis software was employed to select specific regions of interest (ROI) for microstructural parameter analysis (Fig. 5). Subsequently, we conducted a fusion index scoring system to evaluate the degree of fusion: 0,no bone formation; 1,poor new bone formation with clear pseudarthrosis; 2,moderate new bone formation with distinct pseudarthrosis; 3,good new bone formation with possible pseudarthrosis; 4,good new bone formation with potential fusion; 5,clear fusion. Additionally, we used CTvox software to perform 3D bone imaging of the scanned images and observe the morphological changes in the lumbar interbody fusion area. The CTAn bone analysis software was used to quantitatively measure bone growth in the region of interest at the fusion site. The measured parameters included tissue volume (TV), bone volume (BV), bone volume fraction (BV/TV), bone surface area (BS), bone surface-to-bone volume ratio (BS/BV), trabecular thickness (Tb.Th), trabecular spacing (Tb.Sp), trabecular number (Tb.N), and structure model index (SMI).

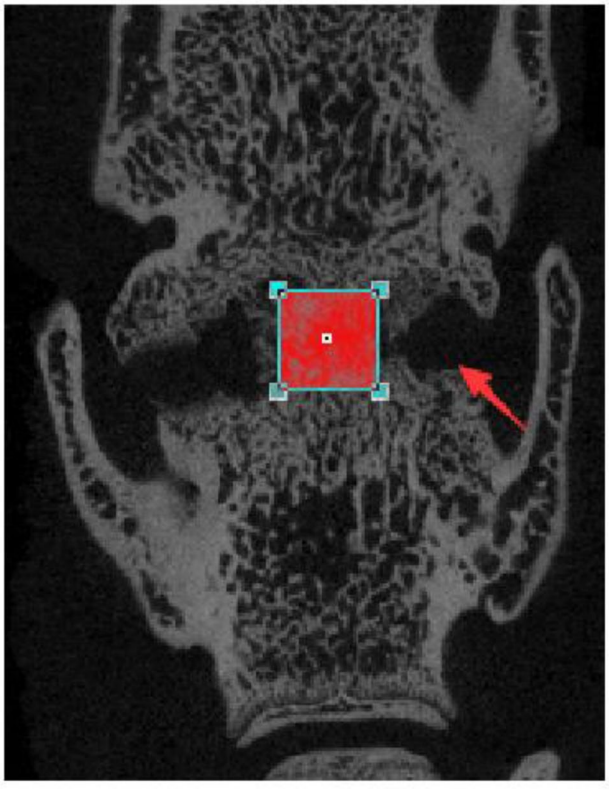

Fig. 5 A small cube with a side length of 2 mm was selected as the region of interest (ROI) at the interbody fusion site, and analysis was performed using CTvox software. The red box indicates the ROI

Histological evaluation

After completing the X-ray examination, the lumbar vertebrae specimens from Groups B, C, and D were decalcified. Once the specimens softened through decalcification, they were trimmed to preserve the fusion gap and a portion of the adjacent vertebral bodies. The trimmed specimens were then embedded in paraffin and sagittal sections were prepared. The sections were stained with HE and Safranin O-Fast Green for light microscopy analysis to assess osteogenesis in the lumbar fusion area. Additionally, immunohistochemical analysis was performed to quantitatively evaluate the expression levels of alkaline phosphatase (ALP), Runx2, and osteopontin (OPN), and and to compare the expression differences of bone-related proteins between groups at 8 weeks post-surgery.

Statistical analysis

Statistical analysis was performed using SPSS version 23.0. Continuous variables are presented as mean ± standard deviation ($x \pm SD$). For continuous data that follow a normal distribution and meet the assumption of homogeneity of variance, one-way analysis of variance (ANOVA) was used for intergroup comparisons. If these assumptions were not met, the Kruskal-Wallis test was applied. Categorical variables are presented as percentages, and intergroup comparisons were performed using the chi-square test or Fisher's exact test. A two-tailed test was used, and a p-value < 0.05 was considered statistically significant.

Results

Important anatomical structures and specific parameters in rats

Through anatomical observation and CT measurements, we identified key anatomical structures for the XLIF approach in lumbar interbody fusion. In SD rats, there are six lumbar vertebrae (L1-L6), with increasing size from L1 to L6. The iliac crest is near L6. The abdominal aorta and inferior vena cava run along the vertebral bodies, with iliac vessels branching off at L5, between the psoas muscle and retroperitoneal fat. The lumbar vertebrae have a triangular cross-section, with wider ends and a narrower center. Transverse processes curve ventrally

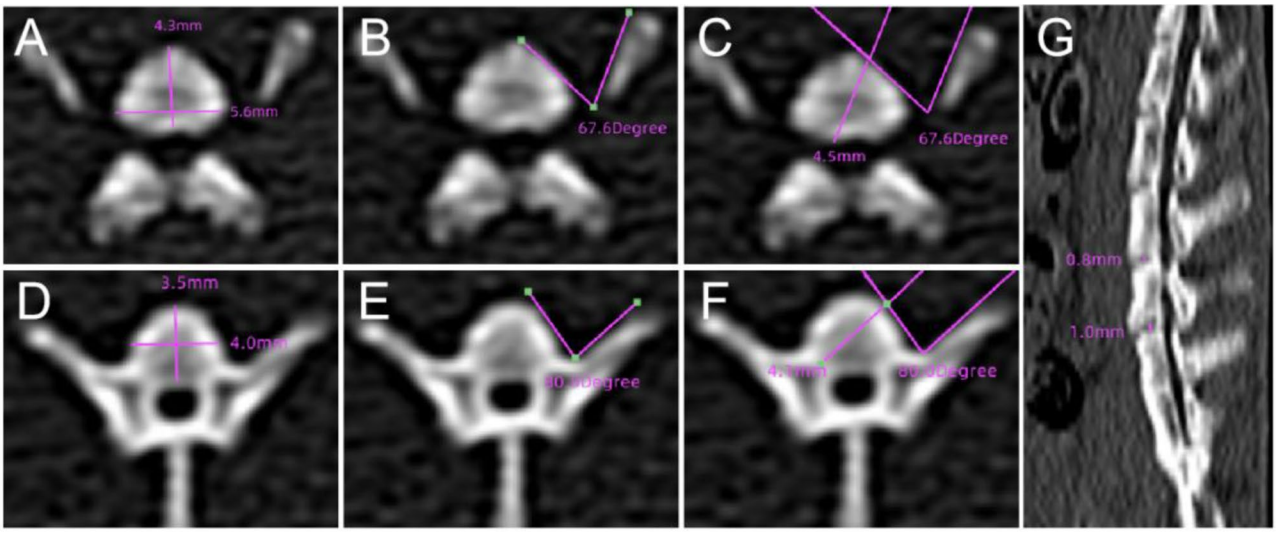

Fig. 6 Measurement of Anatomical Specimens **A**: Sagittal and coronal maximum diameters of the inferior end of L5 vertebra. **B**: Angle between the vertebral body and transverse process at the inferior end of L5 vertebra. **C**: Maximum depth of the screw channel at the inferior end of L5 vertebra. **D**: Sagittal and coronal maximum diameters of the superior end of L6 vertebra. **E**: Angle between the vertebral body and transverse process at the superior end of L6 vertebra. **F**: Maximum depth of the screw channel at the superior end of L6 vertebra. **G**: Height of the intervertebral space between L4 and L6

Table 1 Anatomical data of the rat lumbar spine

	Sagittal maximum diameter	Coronal maximum diameter	Angle between the transverse process and the vertebral body	Lateral length of the vertebral body	Maximum depth of the screw channel
Inferior end of the L4 vertebra	4.0 ± 0.11	5.1 ± 0.17	65.2 ± 3.32	4.1 ± 0.12	4.1 ± 0.06
Superior end of the L5 vertebra	3.4 ± 0.09	3.8 ± 0.11	76.7 ± 4.15	3.0 ± 0.09	3.7 ± 0.07
Inferior end of the L5 vertebra	4.3 ± 0.12	5.5 ± 0.18	67.6 ± 3.49	4.3 ± 0.16	4.5 ± 0.09
Superior end of the L6 vertebra	3.6 ± 0.07	4.1 ± 0.13	85.3 ± 4.48	3.1 ± 0.07	3.9 ± 0.06

and cranially. Vertebral bodies and intervertebral spaces above L4 shrink significantly, with L6 obscured by the iliac crest, making L4-L6 the optimal surgical segments. Using RadiAnt DICOM Viewer, we measured the sagittal and coronal diameters, angle between the vertebral body and transverse process, lateral length, and screw channel depth from L4 to L6 (Fig. 6; Table 1). Based on these measurements, we designed titanium plates (7 mm length, 2.5 mm width, 0.8 mm height) and screws (3 mm length, 1 mm diameter). The screw insertion point was at the anterolateral quadrant, 2 mm from the surgical gap ends, and inserted parallel to the transverse process to avoid nerve damage.

Survival and observational treatment of experimental rats

All animals in Group A survived without postoperative complications. Group B recorded one instance of suture dehiscence with a superficial wound infection; the lesion resolved after debridement and re-suturing. In Group C, one rat developed ipsilateral hind-limb paralysis. Group D experienced two cases of suture dehiscence accompanied by infection, both of which healed after the same treatment.Three peri-operative deaths occurred—none in Groups A and B, two in Group C, and one in Group D. Two fatalities happened intra-operatively owing to severe surgical mishaps: in one animal an improperly angled screw breached the spinal canal, causing cerebrospinal-fluid leakage; in the other, accidental injury to the abdominal aorta led to uncontrollable hemorrhage despite gauze packing, and the rat succumbed to acute massive blood loss.To maintain the prescribed sample size, replacement rats were promptly enrolled and operated upon under identical conditions.

Gross observation and palpation examination

During specimen collection, the surgical segment and adjacent vertebral bodies were preserved. Gross observation revealed varying degrees of bone spur formation at the surgical site in the lumbar spine of Groups B, C, and D. In Groups C and D, the volume of lateral bone spurs was larger and, in some cases, encapsulated the titanium plate, forming a tendency for lateral fusion. The lateral bone spurs enclosed the titanium plate and screw caps. Some of the bone spurs had to be removed to expose the plate and screw caps. Further X-ray evaluation was conducted, and the lateral plate and screws were removed

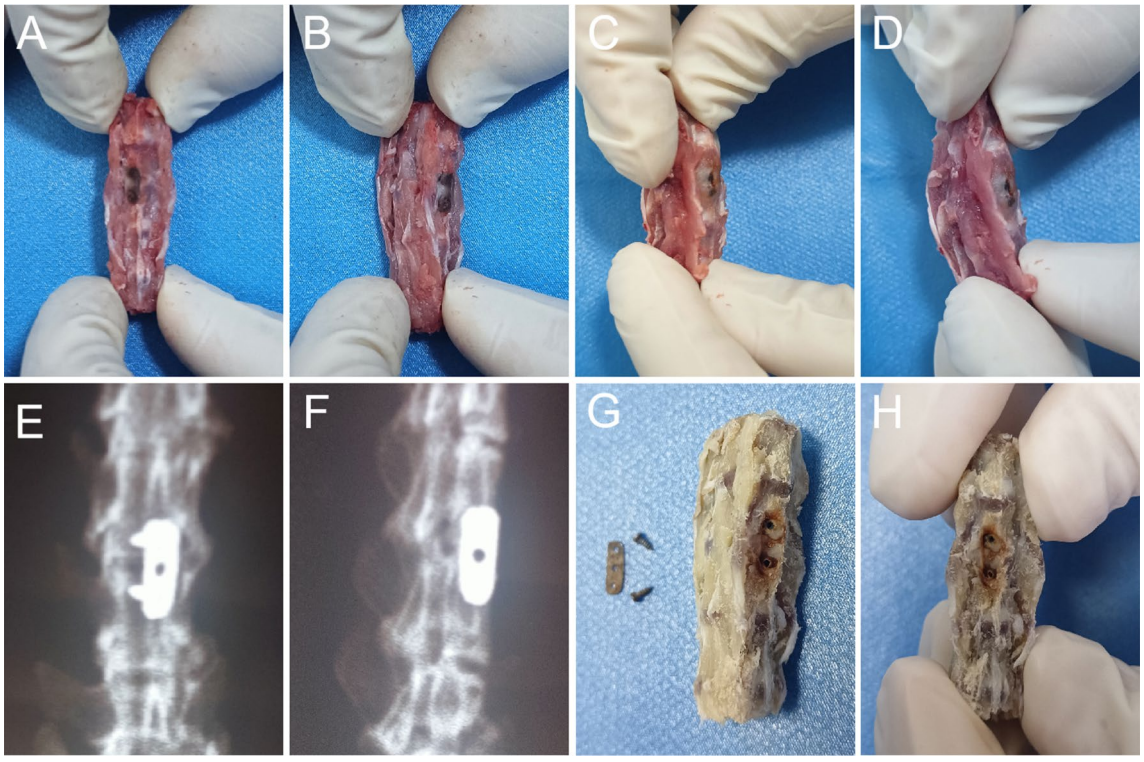

Fig. 7 Gross Observation and Palpation of Rat Specimens After Collection.**A**,**B**:The anteroposterior and lateral views of the specimens show that the titanium plate is encapsulated by bone spurs.**C**,**D**: The specimens in hyperextension and flexion positions show no mobility at the surgical segment. **E**,**F**:X-ray images of the specimens in anteroposterior and lateral views confirm the proper placement of the internal fixation.**G**,**H**: After removal of the internal fixation, good bone bridging is visible between the vertebrae

Table 2 Palpation results of each group

	Group A	Group B	Group C	Group D	*p*
Fusion	1	3	8	11	<0.001*
No fusion	11	9	4	1	

Group A: Control group; **Group B**: Titanium plate fixation group; **Group C**: DBM + Titanium plate fixation group; **Group D**: DBM + CGF + Titanium plate fixation group

* Chi-square test

using a screwdriver (Fig. 7). Upon manual palpation, the fusion rates were as follows: Group A had a fusion rate of 8.3% (1/12), Group B had a fusion rate of 25% (3/12), Group C had a fusion rate of 66.7% (8/12), and Group D achieved a fusion rate of 91.7% (11/12) (Table 2).

Micro-CT examination

During manual palpation, most specimens in Group A exhibited significant intervertebral mobility. Since only the intervertebral space was treated without bone grafting or titanium fixation, this high mobility raised concerns about potential nonfusion between vertebrae. Therefore, we focused on comparing the Micro-CT results from Groups B、C and D. Micro-CT images revealed minimal bone ingrowth in Group B, which had only intervertebral space treatment with lateral fixation. Group C, with DBM implantation and titanium plate fixation, showed significant bone ingrowth but no effective intervertebral connection. Group D, using DBM combined with CGF implantation and titanium plate fixation, exhibited extensive bone ingrowth and robust intervertebral fusion (Fig. 8). Fusion index scores were 2.21 ± 0.51 for Group B, 3.62 ± 0.67 for Group C, and 4.57 ± 0.56 for Group D, with Groups C and D showing significantly higher scores than Group B ($p < .001$). Group D had a significantly higher fusion index score than Group C ($p < .001$). For quantitative bone growth analysis, a 2 mm cube was used to measure tissue volume (TV), bone surface-to-bone volume ratio (BS/BV), and trabecular thickness (Tb.Th) at the intervertebral fusion site (Table 3). The TV measurements showed no significant difference between groups ($p = .494$). The BS/BV ratio was significantly higher in Groups B and C compared to Group D ($p < .001$). Similarly, Tb.Th was significantly higher in Groups B and C than in Group D ($p < .001$). Significant differences were also observed in bone mineral density (BMD), bone volume (BV), bone volume fraction (BV/TV), bone surface area (BS), structure model index (SMI), trabecular number (Tb.N), and trabecular spacing (Tb.Sp), with Group D showing superior values compared to Groups B and C, and Group C outperforming Group B ($p < .001$).

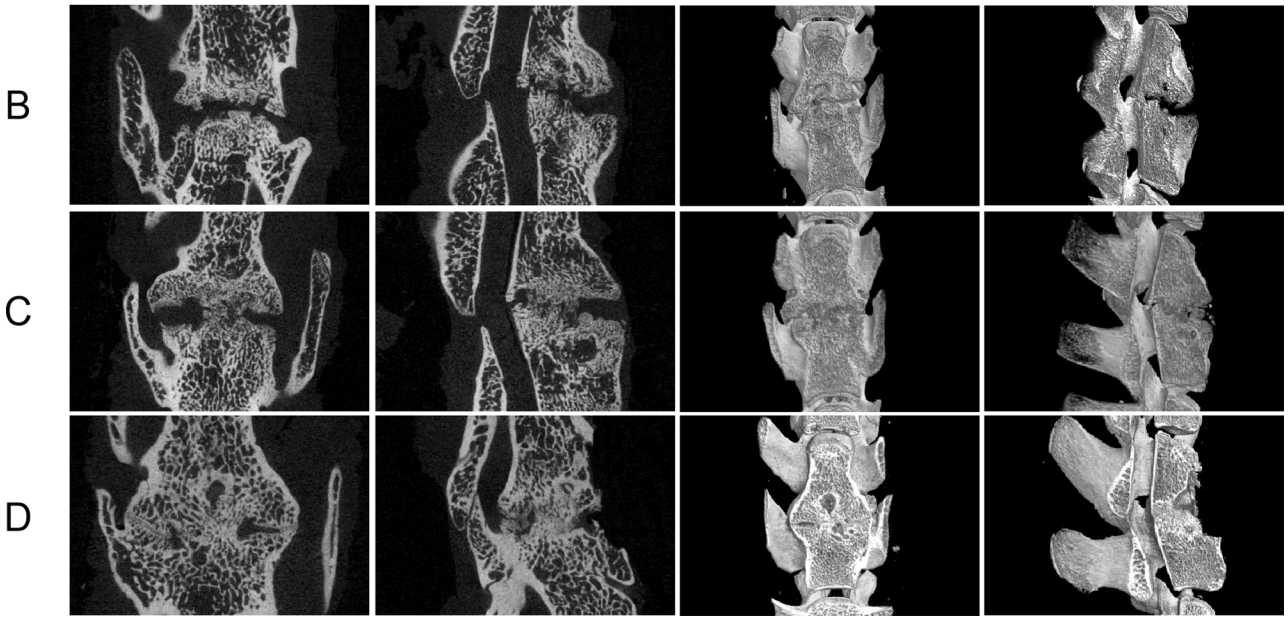

Fig. 8 The Micro-CT images of Groups B, C, and D in the coronal, sagittal, and 3D reconstructions showed that in Group B (Titanium plate fixation), no obvious bony structures were present in the intervertebral space. In Group C (DBM + Titanium plate fixation group), bone ingrowth was observed, but fissures remained at the intervertebral connection. In Group D (DBM + CGF + Titanium plate fixation), significant bone ingrowth was seen across the intervertebral space, forming a stable intervertebral fusion

Table 3 Fusion outcomes under Micro-CT in each group

	B	C	D	*p*
FIS	2.21 ± 0.51a	3.62 ± 0.67b	4.57 ± 0.56c	*P* < .001*
BMD	0.35 ± 0.03a	0.44 ± 0.05b	0.70 ± 0.04c	*P* < .001#
TV	8.18 ± 0.25a	8.08 ± 0.19a	8.06 ± 0.14a	0.494*
BV	2.93 ± 0.23a	4.01 ± 0.49b	6.31 ± 0.73c	*P* < .001*
BV/TV	0.36 ± 0.04a	0.50 ± 0.07b	0.78 ± 0.09c	*P* < .001*
BS	64.74 ± 6.22a	85.67 ± 8.36b	77.00 ± 6.84c	*P* < .001*
BS/BV	22.09 ± 2.13a	21.35 ± 2.09a	12.21 ± 1.09b	*P* < .001*
SMI	0.50 ± 0.07a	0.36 ± 0.06b	0.28 ± 0.04c	*P* < .001*
Tb.Th	0.15 ± 0.02a	0.14 ± 0.02a	0.21 ± 0.03b	*P* < .001*
Tb.N	2.30 ± 0.16a	3.49 ± 0.43b	3.56 ± 0.24c	*P* < .001*
Tb.Sp	0.36 ± 0.04a	0.18 ± 0.02b	0.12 ± 0.02c	*P* < .001#

Group B: Titanium plate fixation. Group C: DBM + Titanium plate fixation group. Group D: DBM + CGF + Titanium plate fixation group. FIS: Fusion index scores; BMD: Bone Mineral Density; TV: Tissue Volume; BV: Bone Volume; BV/TV: Bone Volume Fraction; BS: Bone Surface Area; BS/BV: Bone Surface-to-Bone Volume Ratio; SMI: Structure Model Index; Tb.Th: Trabecular Thickness; Tb.N: Trabecular Number; Tb.Sp: Trabecular Spacing.After data collection, a Shapiro-Wilk test was performed to check the normality of each variable. Based on the results of the normality test, either ANOVA or the Kruskal-Wallis test was used for group comparisons. Multiple comparisons for each variable were performed using the Bonferroni method, and differences between groups were indicated using letter annotations, with groups sharing the same letter indicating no significant difference

* Analysis of variance

#The Kruskal-Wallis test

Histological evaluation

Histopathological examination using HE and Safranin O-Fast Green staining revealed that in Group B, only limited bone formation was observed, with the gap primarily filled by fibrous connective tissue and minimal new cartilage or bone formation. In Group C, more bone formation was present, though some cartilage and fibrous tissue remained. In specimens identified as non-fused by manual palpation, large amounts of fibrous connective tissue and distinct tissue gaps were observed. In Group D, there was minimal fibrous connective tissue, with abundant bone formation, and most vertebrae were effectively bridged, resulting in stable histological fusion (Fig. 9). Immunohistochemical analysis showed significantly higher expression levels of ALP, OPN, and Runx2 in Groups C and D compared to Group B. Furthermore, Group D exhibited significantly higher expression levels of ALP, OPN, and Runx2 than Group C (Fig. 10).

Discussions

This study successfully established a novel rat intervertebral fusion model based on the XLIF surgical technique. By describing the relevant anatomical structures and surgical procedures, and establishing a standardized operation protocol, the model accurately simulates clinical intervertebral fusion. A systematic evaluation was conducted using imaging and histological methods to assess the effects of CGF combined with DBM on intervertebral bone healing. Preliminary results showed that while lateral titanium plate fixation alone provided a certain degree of vertebral stability compared to non-fixation, the bone healing outcomes remained suboptimal. Subsequent micro-CT and histological analyses revealed that DBM combined with titanium plate fixation significantly improved bone formation compared to fixation alone.

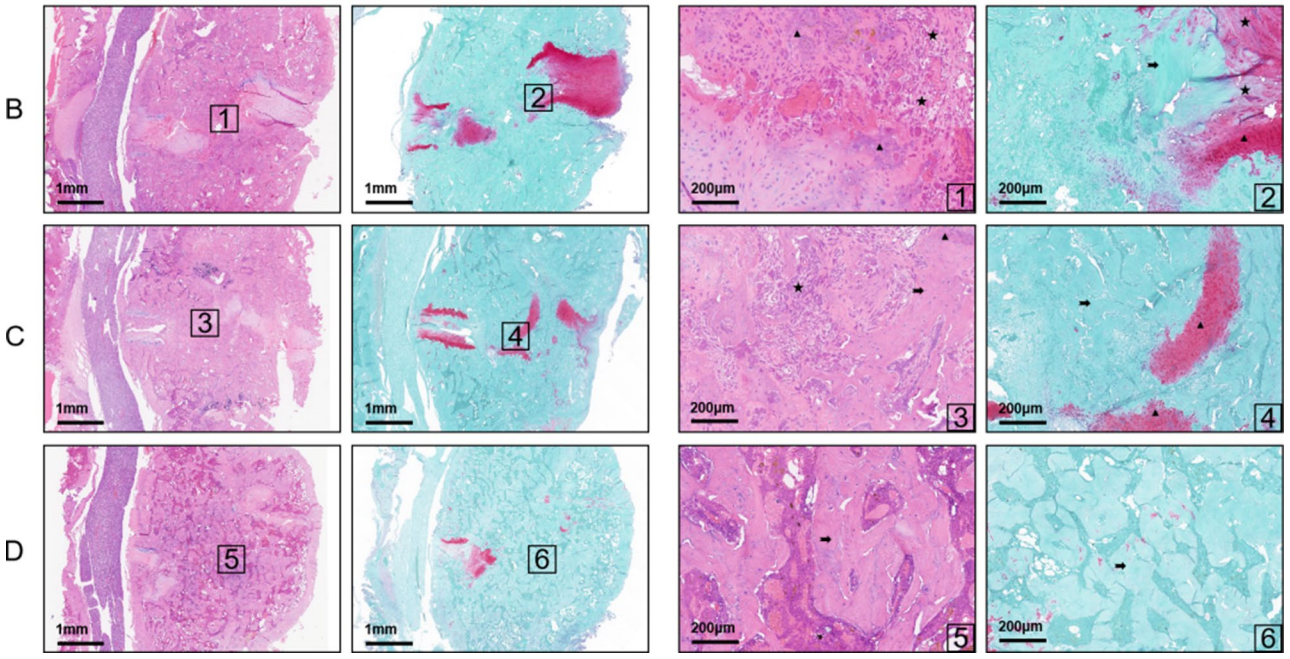

Fig. 9 The histological sections stained with HE and Safranin O-Fast Green from Groups B, C, and D showed bone growth in the fusion areas. Boxes labeled 1 to 6 on the right are magnified. Arrows indicate bone, triangles represent cartilage, and stars represent fibrous connective tissue. The scale bar is shown in the lower left corner of the image. Group B: Titanium plate fixation. Group C: DBM + Titanium plate fixation. Group D: DBM + CGF + Titanium plate fixation

Furthermore, the addition of CGF to DBM resulted in notable increases in fusion rate, microstructural parameters, and the expression of key osteogenic markers such as ALP, Runx2, and OPN. These findings indicate that the combined application of DBM and CGF significantly enhances intervertebral bone healing, and validate the effectiveness and reliability of the novel XLIF rat model in simulating clinical intervertebral fusion.

Over the past century, animal models have been widely used in the study of bone grafts, bone substitutes, growth factors, and gene therapy, offering reproducible and quantifiable data that are difficult to obtain through clinical trials or finite element analysis. Among these models, large animals such as primates, sheep, and pigs have provided critical insights due to their anatomical similarities to humans [16–20]. However, their widespread use is limited by high costs, long experimental cycles, and complex procedures [21, 22]. In contrast, small animal models offer advantages such as lower cost, shorter study duration, and higher reproducibility, making them well-suited for high-throughput screening and mechanistic investigations [23]. As a result, researchers have focused on developing spinal fusion models in small animals like rats. For instance, Raj D. Rao and colleagues established a rat posterolateral lumbar fusion model via the transverse process [24]. However, this model does not address intervertebral disc removal or vertebral fixation, and thus cannot accurately simulate key pathological processes such as disc degeneration or intervertebral stress transmission [25]. Yu-Cheng Yeh et al. introduced a less invasive caudal vertebral fusion model in rats, offering a feasible option for material and mechanical testing [26]. Yu Kang et al. developed an anterior lumbar corpectomy fusion model that more closely mirrors clinical procedures [27]. Despite these efforts, current rat models suffer from significant limitations, including excessive surgical trauma, low reproducibility, and poor representation of the clinical spinal fusion process. To address these gaps, the present study developed a reliable rat interbody fusion model based on the XLIF approach. By incorporating critical steps such as disc removal, internal fixation, and bone grafting, this model closely replicates the clinical fusion procedure. Notably, Japanese scholars have conducted systematic research in the field of rat intervertebral fusion and successfully established an external fixation-based fusion model, with surgical procedures that similarly involve clinically relevant operations such as disc removal, internal fixation, and bone grafting to achieve high clinical fidelity. However, unlike caudal vertebrae models, the lumbar interbody fusion model developed by our team features a larger fusion area. To reduce infection risks, we adopted lateral titanium plate internal fixation while accurately simulating the more complex tissue microenvironment of intervertebral fusion [26, 28]. This innovative platform enables further investigation into the mechanisms of intervertebral fusion and

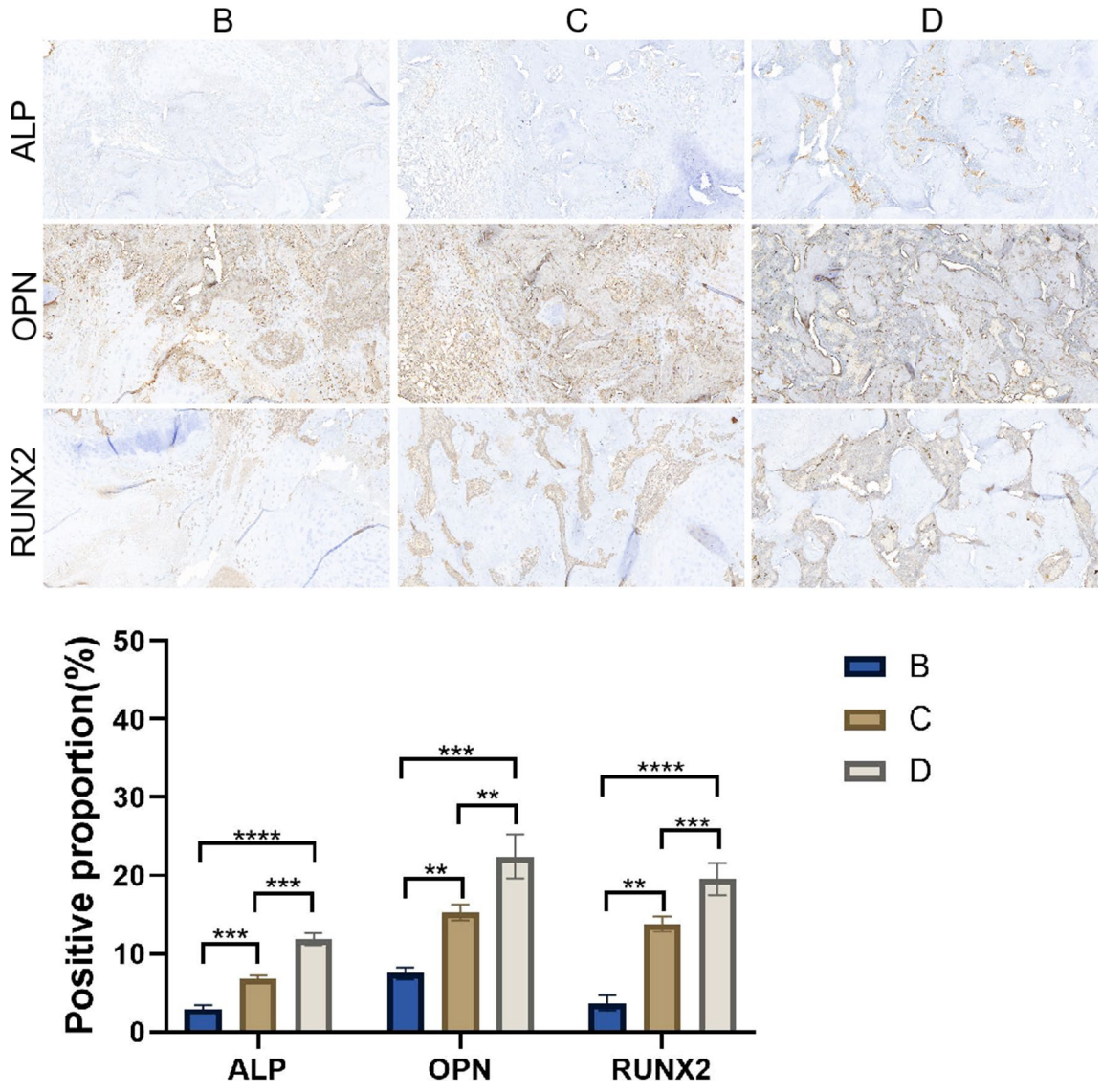

Fig. 10 The figure displays immunohistochemical staining of the osteogenic proteins ALP, OPN, and Runx2 in Groups B, C, and D; the accompanying bar charts quantitatively compare their expression levels across the three groups. It can be observed that in the intervertebral bone implantation groups, C and D, the expression levels of MMP13, OPN, and Runx2 were significantly higher than in the titanium plate fixation group (Group B). Additionally, the expression levels of MMP13, OPN, and Runx2 were notably higher in Group D compared to Group C.Group B: Titanium plate fixation group; Group C: DBM + Titanium plate fixation; Group D: DBM + CGF + Titanium plate fixation

provides a robust foundation for evaluating biomaterials and growth factors in preclinical research. At the same time, due to the small size of rats and the deep anatomical location of the lumbar spine—which is adjacent to multiple vital organs and neurovascular structures—this procedure requires thorough anatomical knowledge and specialized surgical skills. Key technical points for performing XLIF surgery in rats include: (1) Using moist gauze to gently push the peritoneum, retroperitoneal fat, and organs aside during exposure to avoid injury and expand the surgical field; (2) Surgeons should be familiar with the anatomical structures, particularly the inferior vena cava and iliolumbar vessels, for accurate vertebral segment localization; (3) L4-L5 is the preferred surgical level, as the iliac crest obstructs L6; (4) The titanium plate should be placed on the anterior two-thirds of the lateral surface to avoid nerve damage; (5) The lower margin of the lumbar vertebrae forms a step-like structure, so partial removal of the upper vertebra's lower edge may be needed; (6) The screw insertion point should be in the lateral half of the anterior vertebral body surface, with the screw parallel to the transverse process to avoid obstruction and ensure a long screw trajectory, reducing the risk of spinal canal breach.

CGF is a third-generation autologous platelet concentrate that offers significant improvements over the earlier

forms, PRP and PRF, particularly in terms of growth factor concentration and sustained release. PRP, as the first-generation product, is obtained by centrifuging blood to concentrate platelets, followed by the addition of activators such as calcium chloride or thrombin to induce the release of growth factors. It has been mainly used to promote tissue repair [29]. However, research indicates that most growth factors in PRP are released within the first 24 h, making it difficult to provide prolonged biological stimulation, which limits its effectiveness in long-term bone healing [30, 31]。 To address these limitations, PRF was introduced by Choukroun in 2001 as a second-generation platelet concentrate [32]. PRF forms a dense fibrin matrix through a natural coagulation process without the need for external activators. This matrix effectively traps a high concentration of platelets and leukocytes, offering better sustained release of growth factors and longer-lasting biological effects. PRF has been widely used in wound healing, burn treatment, dentistry, and the management of osteoarthritis [33, 34]. Nevertheless, some studies have pointed out that the fibrin network in PRF is relatively loose, and the concentration of growth factors is lower compared to other preparations. These characteristics limit its clinical effectiveness in bone fusion [35]. In 2006, Sacco [15] developed CGF using a variable-speed centrifugation technique to overcome the shortcomings of PRP and PRF. This method mechanically activates platelet al.pha granules through controlled acceleration and deceleration, producing an autologous concentrate that contains higher levels of growth factors and CD34-positive cells. CGF is rich in key growth factors such as TGF-β, VEGF, and PDGF, which play essential roles in bone repair, soft tissue regeneration, and angiogenesis. Compared with PRP and PRF, CGF not only provides a higher concentration of growth factors but also forms a denser fibrin matrix that supports more effective sustained release. Studies have shown that the unique three-dimensional fibrin scaffold of CGF can prolong the release of growth factors for up to 14 days [35, 36]. Due to its high osteoinductive potential and dense osteoconductive structure, CGF has been increasingly applied in fields such as dentistry, oral and maxillofacial surgery, and orthopedics, particularly in situations requiring bone regeneration and tissue integration [37, 38].

Previous studies have demonstrated that CGF is capable of inducing osteogenic differentiation in bone marrow mesenchymal stem cells under in vitro conditions [39, 40]. Animal studies further demonstrate that CGF promotes the formation of dense, mature bone tissue [41]. Masuki et al. [42]reported that both CGF and PRF outperform PRP in stimulating the proliferation of human periosteal cells. In another comparative study, Park et al. [37]found that CGF exhibited greater regenerative potential than PRF during the early stages of bone formation in femoral defects. Despite its strong osteoinductive capacity, CGF alone may not fully meet the complex demands of clinical bone healing, particularly in environments requiring both osteoinduction and osteoconduction. As such, combining CGF with materials that offer strong osteoconductive properties has emerged as a promising strategy to improve spinal fusion outcomes. DBM is a widely used bone graft material in spinal surgery, commonly applied in intervertebral fusion procedures [43]. Through demineralization, DBM retains the organic components of bone, including collagen, glycosaminoglycans, and a variety of osteogenic factors such as bone morphogenetic proteins (BMPs). These elements provide a structural framework for bone regeneration and play an important role in osteoconduction during healing [44]. However, while DBM has good osteoconductive properties, its osteoinductive potential is limited—particularly in poorly vascularized environments or in cases requiring long healing periods, such as spinal interbody fusion. As a result, DBM alone may not be sufficient to ensure successful fusion. CGF, on the other hand, is rich in osteoinductive growth factors including PDGF, TGF-β, VEGF, IGF-1 and BMPs. These factors provide sustained biological stimulation that supports local bone healing. Therefore, we hypothesize that the osteoconductive scaffold provided by DBM and the osteoinductive stimulus from CGF can act synergistically. When used together, DBM serves as a physical matrix for cell adhesion and migration, while CGF delivers growth factors in a sustained manner, activating osteoblasts and promoting angiogenesis. This combination is expected to accelerate new bone formation and enhance the overall fusion process.

To evaluate the effect of combining DBM with CGF on intervertebral bone healing, we conducted a preliminary study using a novel rat interbody fusion model. Manual palpation performed eight weeks postoperatively revealed a fusion rate of 91.7% in Group D (DBM + CGF), compared to a significantly lower rate of 66.7% in Group C, which received DBM alone. These findings were further supported by micro-CT analysis, which demonstrated that the combination of DBM and CGF substantially improved the quality of bone healing. Group D exhibited clear intervertebral bone bridging, along with superior metrics in bone volume, total bone mass, and bone surface area compared to Groups B and C. Histological assessment also confirmed more robust and stable bone fusion in Group D, whereas Groups B and C showed varying degrees of fibrous connective tissue within the intervertebral space. Immunohistochemical analysis revealed significantly higher expression levels of key osteogenic markers—including ALP, Runx2 and OPN—in Group D compared to Group C. These results further validated that the diverse growth factors present in CGF enhance the expression of osteogenesis-related

proteins. Taken together, the data suggest that the combined application of DBM and CGF exerts a strong osteoinductive effect, accelerating new bone formation and promoting more effective intervertebral fusion.

Based on the combined findings from manual palpation, micro-CT analysis, histological evaluation, and immunohistochemistry, this study demonstrates that the use of DBM in combination with CGF holds significant promise as an alternative bone grafting strategy in intervertebral fusion procedures. DBM offers a stable osteoconductive scaffold, while CGF, rich in multiple osteoinductive growth factors, enhances local osteogenesis and angiogenesis through its sustained-release properties.The synergistic effect of these two materials not only increased the fusion rate but also significantly improved bone quality in the rat XLIF interbody fusion model, which closely mimics clinical surgical conditions. Importantly, this approach eliminates the need for autologous bone harvesting, thereby avoiding common donor site complications and addressing the issue of limited graft availability. These results provide a strong experimental foundation for future translational research and support the clinical potential of DBM combined with CGF as a viable substitute for autologous bone in spinal fusion surgeries.

Certainly, this study also has some limitations: (1)The study included only an 8-week follow-up period, which may have been insufficient to fully observe bone healing, long-term fusion stability, and the later stages of bone remodeling. (2)The evaluation of spinal fusion primarily relied on imaging, histology, and manual palpation, without incorporating quantitative biomechanical testing, which limits the assessment of functional strength. (3)The current investigation did not systematically investigate different dosages, mixing ratios, or the release profile of growth factors in CGF, which limits the ability to determine the optimal combination strategy and understand its underlying mechanisms. (4)Theoretically, to align with clinical practice, CGF should be prepared using autologous blood. However, due to the limited blood volume in rats, allogeneic blood had to be used. (5)The control group in this study did not include an autograft group. To further evaluate the effect of CGF combined with DBM on intervertebral fusion, we will incorporate an autograft group in future studies to verify whether the combination of CGF and DBM can achieve fusion outcomes comparable to autologous bone grafting. (6)Each group in this study included only 12 rats, representing a relatively small sample size. Future investigations will expand the cohort and extend the follow-up period to further test and strengthen the reliability and robustness of our findings. (7)This study was conducted using a small animal model, and due to limitations such as the size of the intervertebral gap, biomechanics, and other physiological differences, these findings may require cautious validation and further research when extrapolated to clinical practice.

Conclusion

This study successfully established a reliable novel rat XLIF interbody fusion model and, for the first time, systematically evaluated the efficacy of combining DBM with CGF in promoting intervertebral fusion. The results demonstrated that the addition of CGF significantly enhanced the osteogenic potential of DBM. Compared to DBM alone, the combination yielded superior outcomes in terms of fusion rate, bone microstructural parameters, and the expression of osteogenesis-related proteins. Without the need for autologous bone grafting, the synergy between CGF and DBM effectively promoted bone healing through both osteoinductive and osteoconductive mechanisms. These findings suggest that DBM combined with CGF may offer a promising clinical alternative to reduce the reliance on autologous bone grafts.

Abbreviations

DBM	Demineralized bone matrix
CGF	Concentrated growth factors
XLIF	Extreme lateral interbody fusion
FIS	Fusion index scores
PRP	Platelet-rich plasma
PRF	Platelet-rich fibrin
SD	Sprague-Dawley
ROI	Specific regions of interest
ALP	Alkaline phosphatase
OPN	Osteopontin
TV	Tissue volume
BV	Bone volume
BV/TV	Bone volume fraction
BS	Bone surface area
BS/BV	Bone surface-to-bone volume ratio
Tb.Th	Trabecular thickness
Tb.Sp	Trabecular spacing
Tb.N	Trabecular number
SMI	Structure model index

Acknowledgements

Not applicable.

Author contributions

Wei Zhang is responsible for concept and design. Han Wu and Shaorong Li are responsible for data collection and analysis. Han Wu is responsible for drafting of the article. Weijian Wang are responsible for critical revision of the article. Han Wu are responsible for important intellectual content. Han Wu and Shaorong Li revised and polished the manuscript. Wei Zhang is responsible for study supervision. All the authors approved the final article.

Funding

The authors thankfully acknowledge the financial support listed below: S&T Program of Hebei 22377708D; Hebei Provincial Government funded Provincial Medical Talent Project in 2022; 2023 Hebei Medical University "14th Five-Year Plan" Clinical Medical Innovation Research Team.

Data availability

No datasets were generated or analysed during the current study.

Declarations

Ethics approval and consent to participate
All studies have been performed in accordance with the ethical standards in the 1964 Declaration of Helsinki and the relevant regulations of the US Health Insurance Portability and Accountability Act (HIPAA). This experiment obtained ethical approval from the Ethics Committee of the Third Hospital of Hebei Medical University (No. Z2023-026-1).

Consent for publication
Not applicable.

Competing interests
The authors declare no competing interests.

Author details
[1]Department of Spine Surgery, The Third Hospital of Hebei Medical University, 139 Ziqiang Street, Shijiazhuang, Hebei 050031, China

Received: 10 April 2025 / Accepted: 22 May 2025
Published online: 27 May 2025

References

1. Schnake KJ, Rappert D, Storzer B, Schreyer S, Hilber F, Mehren C. Lumbale Spondylodese– Indikationen und techniken. Orthopäde. 2018;48(1):50–8.
2. Wong AXJ, Tang DH, Kaliya-Perumal A-K, Oh JY-L. The evolution of lateral lumbar interbody fusion: A journey from past to present. Medicina. 2024;60(3):378.
3. Berjano P, Gautschi OP, Schils F, Tessitore E. Extreme lateral interbody fusion (XLIF®): how I do it. Acta Neurochir. 2014;157(3):547–51.
4. Li JXJ, Phan K, Mobbs R. Oblique lumbar interbody fusion: technical aspects, operative outcomes, and complications. World Neurosurg. 2017;98:113–23.
5. Liu X, Zhou J, Chen M, Chen S, You J, Li Y, Lv H, Zhang Y, Zhou Y. 3D-printed biomimetic bone scaffold loaded with lyophilized concentrated growth factors promotes bone defect repair by regulation the VEGFR2/PI3K/AKT signaling pathway. Int J Biol Macromol. 2024;282(Pt 2):136938.
6. Plantz MA, Minardi S, Lyons JG, Greene AC, Ellenbogen DJ, Hallman M, Yamaguchi JT, Jeong S, Yun C, Jakus AE, et al. Osteoinductivity and Biomechanical assessment of a 3D printed demineralized bone matrix-ceramic composite in a rat spine fusion model. Acta Biomater. 2021;127:146–58.
7. Myeroff C, Archdeacon M. Autogenous bone graft: donor sites and techniques. J Bone Joint Surg. 2011;93(23):2227–36.
8. Bai L, Zhang X, Shen W, Wang P, Yin X, Liu J, Xu H, Liu B, Man Z, Li W. Multifunctional scaffold comprising Metal–Organic framework, hydrogel, and demineralized bone matrix for the treatment of Steroid-Induced femoral head necrosis. Small. 2024;21(3):e2407758.
9. Driscoll JA, Lubbe R, Jakus AE, Chang K, Haleem M, Yun C, Singh G, Schneider AD, Katchko KM, Soriano C, et al. 3D-Printed Ceramic-Demineralized bone matrix hyperelastic bone composite scaffolds for spinal fusion. Tissue Eng Part A. 2020;26(3–4):157–66.
10. Kawase T, Tanaka T. An updated proposal for terminology and classification of platelet-rich fibrin. Regenerative Therapy. 2017;7:80–1.
11. Dohan Ehrenfest DM, Pinto NR, Pereda A, Jiménez P, Corso MD, Kang B-S, Nally M, Lanata N, Wang H-L, Quirynen M. The impact of the centrifuge characteristics and centrifugation protocols on the cells, growth factors, and fibrin architecture of a leukocyte- and platelet-rich fibrin (L-PRF) clot and membrane. Platelets. 2017;29(2):171–84.
12. Huang L, Zou R, He J, Ouyang K, Piao Z. Comparing osteogenic effects between concentrated growth factors and the acellular dermal matrix. Brazilian Oral Res. 2018;32(0):e29.
13. Wang F, Li Q, Wang Z. A comparative study of the effect of Bio-Oss® in combination with concentrated growth factors or bone marrow-derived mesenchymal stem cells in canine sinus grafting. J Oral Pathol Med. 2016;46(7):528–36.
14. Drespe IH, Polzhofer GK, Turner AS, Grauer JN. Animal models for spinal fusion. Spine J. 2005;5(6):S209–16.
15. Rodella LF, Favero G, Boninsegna R, Buffoli B, Labanca M, Scarì G, Sacco L, Batani T, Rezzani R. Growth factors, CD34 positive cells, and fibrin network analysis in concentrated growth factors fraction. Microsc Res Tech. 2011;74(8):772–7.
16. Yamada K, Ito M, Akazawa T, Murata M, Yamamoto T, Iwasaki N. A preclinical large animal study on a novel intervertebral fusion cage covered with high porosity titanium sheets with a triple pore structure used for spinal fusion. Eur Spine J. 2015;24(11):2530–7.
17. Arunakul R, Anumas S, Pattharanitima P, Susrivaraput C, Pholsawatchai W. Unilateral biportal endoscopic versus microscopic transforaminal lumbar interbody fusion for lumbar degenerative disease: a retrospective study. J Orthop Surg Res. 2024;19(1):326.
18. Wang W, Cui Y, Sun X, Zhang H, Yin W, Cui X, Jiao W. Transforaminal posterior lumbar interbody fusion microscopic safe operating area: a three-dimensional model study based on computed tomography imaging. J Orthop Surg Res. 2024;19(1):342.
19. Guo W, Ye J, Li T, Yu Y, Fan X. Evaluation of the learning curve and complications in unilateral biportal endoscopic transforaminal lumbar interbody fusion: cumulative sum analysis and risk-adjusted cumulative sum analysis. J Orthop Surg Res. 2024;19(1):194.
20. Bahir AW, Daxing W, Jiayu X, Bailian L, Shao G. Comparative efficacy and fusion outcomes of unilateral bi-portal endoscopic transforaminal lumbar interbody fusion versus minimally invasive transforaminal lumbar interbody fusion in treating single-segment degenerative lumbar spondylolisthesis with lumbar spinal stenosis: a two-year retrospective study. J Orthop Surg Res. 2024;19(1):835.
21. Gu Y, Zhang F, Lineaweaver WC, Zhang J, Jia L, Qi J, Wang J, Zhen X. In vivo study of Hydroxyapatite-coated hat type cervical intervertebral fusion cage combined with IGF-I and TGF-β1 in the goat model. Clin Spine Surgery: Spine Publication. 2016;29(5):E267–75.
22. Cunningham ME, Kelly NH, Rawlins BA, Boachie-Adjei O, van der Meulen MCH, Hidaka C. Lumbar spine intervertebral disc gene delivery of BMPs induces anterior spine fusion in Lewis rats. Sci Rep. 2022;12(1):16847.
23. Gruber HE, Gordon B, Williams C, Ingram JA, Norton HJ, Hanley EN. A new small animal model for the study of spine fusion in the sand rat: pilot studies. Lab Anim. 2009;43(3):272–7.
24. Rao RD, Bagaria VB, Cooley BC. Posterolateral intertransverse lumbar fusion in a mouse model: surgical anatomy and operative technique. Spine J. 2007;7(1):61–7.
25. Yeh Y-C, Yang C-C, Tai C-L, Tsai T-T, Lai P-L, Fu T-S, Niu C-C, Chen L-H, Chen W-J. Characterization of a novel caudal vertebral interbody fusion in a rat tail model: an implication for future material and mechanical testing. Biomedical J. 2017;40(1):62–8.
26. Okada R, Kaito T, Ishiguro H, Kushioka J, Otsuru S, Kanayama S, Bal Z, Kitaguchi K, Hashimoto K, Makino T, et al. Assessment of effects of rhBMP-2 on interbody fusion with a novel rat model. Spine J. 2020;20(5):821–9.
27. Kang Y, Liu C, Wang M, Wang C, Yan Y-G, Wang W-J. A novel rat model of interbody fusion based on anterior lumbar corpectomy and fusion (ALCF). BMC Musculoskelet Disord. 2021;22(1):965.
28. Nakagawa S, Okada R, Kushioka J, Kodama J, Tsukazaki H, Bal Z, Tateiwa D, Ukon Y, Hirai H, Makino T, et al. Effects of rhBMP-2-loaded hydroxyapatite granules/beta-tricalcium phosphate hydrogel (HA/β-TCP/hydrogel) composite on a rat model of caudal intervertebral fusion. Sci Rep. 2022;12(1):7906.
29. Wang Q, Huang Z, Huang X, Zhang T, Wang W. Reparative effect of super active platelet combined with allogeneic bone for large bone defects. Artif Organs. 2021;45(10):1219–28.
30. Taçyıldız AE, İnceoğlu F. Classification of osteophytes occurring in the lumbar intervertebral foramen. Tomography. 2024;10(4):618–31.
31. Liu W, Huang Y, Liu D, Zeng T, Wang J, Li A, Wang D, Wang X. The combination of platelet rich plasma gel, human umbilical mesenchymal stem cells and nanohydroxyapatite/polyamide 66 promotes angiogenesis and bone regeneration in large bone defect. Tissue Eng Regenerative Med. 2022;19(6):1321–36.
32. Dohan DM, Choukroun J, Diss A, Dohan SL, Dohan AJJ, Mouhyi J, Gogly B. Platelet-rich fibrin (PRF): A second-generation platelet concentrate. Part III: leucocyte activation: A new feature for platelet concentrates? *Oral surgery, oral medicine, oral pathology*. Oral Radiol Endodontology. 2006;101(3):e51–5.
33. Varghese MP, Manuel S, Kumar L, K S. Potential for osseous regeneration of Platelet-Rich Fibrin—A comparative study in mandibular third molar impaction sockets. J Oral Maxillofac Surg. 2017;75(7):1322–9.
34. Agrawal AA. Evolution, current status and advances in application of platelet concentrate in periodontics and implantology. World J Clin Cases. 2017;5(5):159–71.
35. Lei L, Yu Y, Han J, Shi D, Sun W, Zhang D, Chen L. Quantification of growth factors in advanced platelet-rich fibrin and concentrated growth factors

and their clinical efficacy as adjunctive to the GTR procedure in periodontal intrabony defects. J Periodontol. 2019;91(4):462–72.
36. Wang L, Wan M, Li Z, Zhong N, Liang D, Ge L. A comparative study of the effects of concentrated growth factors in two different forms on osteogenesis in vitro. Mol Med Rep. 2019;20(2):1039–48.
37. Park H-C, Kim S-G, Oh J-S, You J-S, Kim J-S, Lim S-C, Jeong M-A, Kim J-S, Jung C, Kwon Y-S, et al. Early bone formation at a femur defect using CGF and PRF grafts in adult dogs. Implant Dent. 2016;25(3):387–93.
38. Li H, Zhang X, Ameer KA, Zhang X, Du W, Mei S, Li X. Clinical observation of concentrated growth factor (CGF) combined with Iliac cancellous bone and composite bone material graft on postoperative osteogenesis and inflammation in the repair of extensive mandibular defects. J Stomatology Oral Maxillofacial Surg. 2023;124(6):101472.
39. Chen X, Wang J, Yu L, Zhou J, Zheng D, Zhang B. Effect of concentrated growth factor (CGF) on the promotion of osteogenesis in bone marrow stromal cells (BMSC) in vivo. Sci Rep. 2018;8(1):5876.
40. Rochira A, Siculella L, Damiano F, Palermo A, Ferrante F, Carluccio MA, Calabriso N, Giannotti L, Stanca E. Concentrated growth factors (CGF) induce osteogenic differentiation in human bone marrow stem cells. Biology. 2020;9(11):370.
41. Cui Z, Zhou L, Huang J, Xu L, Ding Z, Hu H, Cao X, Zhao M, Wu S. Dual-model biomanufacturing of porous biomimetic scaffolds with concentrated growth factors and embedded endothelial vascular channels for bone defect regeneration. Chem Eng J. 2024;483:148933.
42. Masuki H, Okudera T, Watanebe T, Suzuki M, Nishiyama K, Okudera H, Nakata K, Uematsu K, Su C-Y, Kawase T. Growth factor and pro-inflammatory cytokine contents in platelet-rich plasma (PRP), plasma rich in growth factors (PRGF), advanced platelet-rich fibrin (A-PRF), and concentrated growth factors (CGF). Int J Implant Dentistry. 2016;2(1):19.
43. Zadegan SA, Abedi A, Jazayeri SB, Vaccaro AR, Rahimi-Movaghar V. Demineralized bone matrix in anterior cervical discectomy and fusion: a systematic review. Eur Spine J. 2016;26(4):958–74.
44. Gruskin E, Doll BA, Futrell FW, Schmitz JP, Hollinger JO. Demineralized bone matrix in bone repair: history and use. Adv Drug Deliv Rev. 2012;64(12):1063–77.

Publisher's note